Int J Clin Exp Med 2017;10(12):16381-16387
www.ijcem.com /ISSN:1940-5901/IJCEM0057876

Original Article

Spectral CT imaging improve the differentiation of lymph node metastasis from different tumors

Jingang Liu[1*], Weiguang Shao[1*], Yu Han[1], Xizhen Wang[1], Xingsheng Zhao[1], Lixin Li[1], Wenjuan Wang[2], Bin Wang[1,3]

[1]*Imaging Center of Affiliated Hospital, Weifang Medical University, Weifang 261031, China;* [2]*Department of Radiology, Weifang People's Hospital, Weifang 261041, China;* [3]*Department of Medical Imaging and Nuclear Medicine, Binzhou Medical University, Yantai, China.* [*]*Equal contributors.*

Received November 14, 2015; Accepted November 6, 2017; Epub December 15, 2017; Published December 30, 2017

Abstract: Purpose: To investigate the feasibility of differentiating metastatic lymph nodes from lymphoma, lung adenocarcinoma, and lung squamous cell carcinoma using spectral CT imaging. Methods: 64 patients with malignant tumors and an associated 256 metastatic lymph nodes underwent spectral CT imaging during the arterial phase. Eleven sets of monochromatic images with energy levels from 40-140 keV with 10 keV intervals, and material decomposition images using iodine and water as the base material pair were reconstructed and analyzed from the spectral CT imaging during the arterial phase. The iodine and water contents were measured in the iodine and water-based images, respectively. Results: The highest contrast-noise-ratio values for the lymph nodes were obtained at the 70 keV image setting. The CT attenuation values of metastatic lymph nodes at the 11 keV levels were different from each other ($P < 0.05$). The iodine content of metastatic lymph nodes from lymphoma was 1.93±0.04 mg/mL, which was different from that of lung adenocarcinoma (1.16±0.15 mg/mL) and lung squamous cell carcinoma (1.25±0.21 mg/mL) (all $P < 0.001$). There was no significant difference for their water contents: 1029.40±20.85 mg/mL from lymphoma, 1024.98±11.19 mg/mL from lung adenocarcinoma, and 1022.12±12.94 mg/mL from lung squamous cell carcinoma ($P > 0.05$). Conclusions: Spectral CT imaging is a promising method for distinguishing metastatic lymph nodes from different malignant tumors using CT attenuation values at different photon energy levels and iodine content measurements.

Keywords: Lymph nodes, neoplasm metastasis, tomography, X-ray computed, spectral CT imaging

Introduction

The spectral imaging technique gives Gemstone CT the power to obtain spectral images. Gemstone spectral imaging (GSI) broke through the limitations of conventional CT, which only has single parametric imaging. GSI makes material differentiation with monochromatic energy feasible [1]. A dual-energy CT can acquire two-energy images in the same location. Gemstone spectral imaging provides a serial kVp ranging from 40 to 140 kVp and an attenuation curve that displays the attenuation of any tissue across the kVp range. The linear attenuation coefficient of different tissue decreases with an increase of kVp. Different tissue has its own rate of decline, which will enhance the contrast between two different tissues at selected kVp [2]. Monochromatic spectral images generated by GSI range from 40 to 140 kVp providing more details of tissues [3-5]. According to these monochromatic images ranged from 40 to 140 kVp, the contrast-to-noise ratio (CNR), signal-to-noise ratio (SNR) and noise level of background can be optimized [6]. Based on anatomic images, spectral imaging can analyze the tissue component by way of poly-chromatophilic images, such as the monochromatic imaging, iodine-based imaging, water-based imaging and calcium-based imaging. The attenuation curve of GSI has the potential to show the physical character of different tissues. So, GSI plays an important role in CT studies transferring from the macro level to the micro level of the body. Spectral computed tomography has been used to differentiate benign and malignant tumors [7-9].

Metastatic lymph nodes are a common metastatic pattern with malignant tumors, and a key

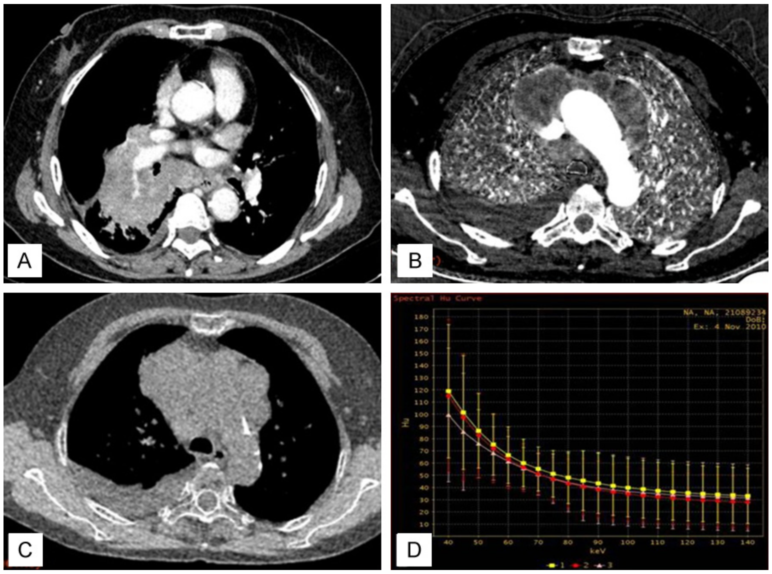

Figure 1. A 50-year-old male with lymphoma. (A) is an enhanced axial monochromatic image of the abdomen showing large and fused lymph nodes surrounding the aorta and vena cava in the retroperitoneal space. (B) and (C) are an iodine based image and a water-based image. Fused lymph nodes surrounding the aorta and vena cava are more obvious on the iodine-based image than on the water-based image. (D) is the spectrum curve of lymph node showing similar curves of three ROIs lymphoma. The shapes of these spectrum curves are similar to each other.

indicator of recurrence. In some malignant tumors, lymph node metastases may be found earlier, even before the original tumor is detected using imaging modalities [10-13]. Therefore, detecting and differentiating metastatic lymph nodes plays an important role in tumor staging. However, with conventional CT, the size, shape, and CT value of lymph node were used to identify benign and malignant lymph nodes [14-16]. In these cases, the sensitivities and specificities of conventional CT in detecting metastatic lymph nodes ranged only from 52% to 66% and from 69% to 93%, respectively. The low sensitivity and high false-negative rate of conventional CT limited the usage in N-stage of lung cancer [17-20]. The recently introduced dual energy spectral CT imaging with the rapid tube voltage switch between the low kVp (80 kVp) and high kVp (140 kVp) during a single rotation is capable of generating monochromatic image sets with photon energy levels from 40 keV to 140 keV to provide better contrast resolution and a unique CT attenuation curve as a function of photon energy (spectral HU curve) and material decomposition images to provide material separation. The metastatic lymph nodes have similar biological features to their primary malignant tumors. The cellularity, proliferative ratio, angiogenesis and tissue density in CT of malignant neoplasms were usually different from each other [10-13]. So, we hypothesize that metastatic lymph nodes from different malignant tumors may have inherently unique spectral HU curves. The purpose of our study was to evaluate the feasibility of using dual energy spectral CT to differentiate metastatic lymph nodes from different malignant tumors.

Material and methods

Subjects

Protocols and informed consent provisions were reviewed and approved by Wei fang Medical University Review Board. Sixty four patients with malignant tumor were enrolled in our study. There were thirty five males and twenty nine females with an average age of 59 years old (ages from 48 to 77 years). Eighteen of them had lymphoma (Ly) with 72 lymph nodes involved. Twenty four had lung adenocarcinoma (LAC) with 96 lymph nodes involved. The other twenty-two had lung squamous cell carcinoma (LSC) with 88 lymph nodes involved. All the malignancies were confirmed by pathological examination.

CT scanning protocol and data post-process

Pre-contrast scan and enhanced scans in the arterial phase and venous phase were performed using a GE high-definition CT scanner (Discovery CT750 HD, GE Healthcare, USA). The contrast medium Iohexol (Urich, Germany) was injected using a high pressure injector at the rate of 3.0 ml/sec via the right ulnar vein. The scan start time for the arterial phase and venous phase was 30 seconds and 55 seconds after injection, respectively. The pre-contrast scan and contrast-enhanced scan in the portal venous phase were carried out using the conventional helical scan mode with the following

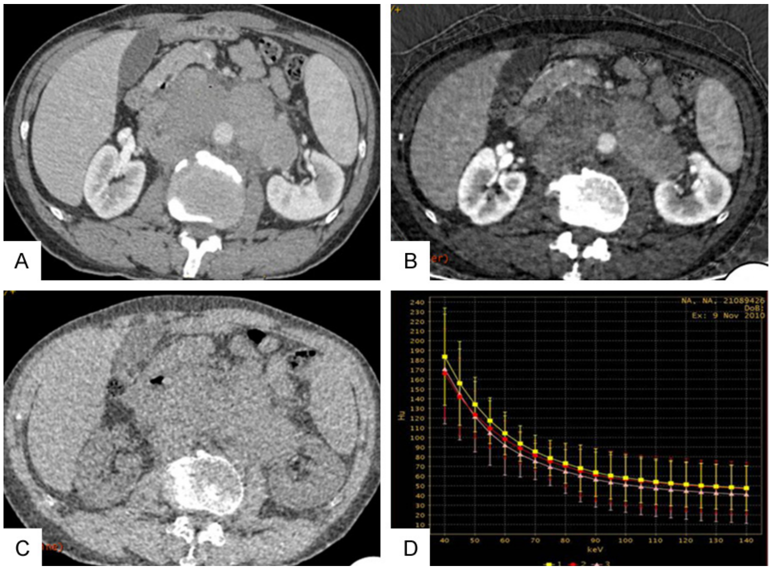

Figure 2. A 66 year old female with LSC. (A) is an enhanced axial monochromatic image of chest showing a large and fused mass in the right hailer. (B) and (C) are an iodine-based image and a water-based image showing the metastatic lymph nodes. Metastatic lymph nodes are more obvious on the iodine-based image than on the water-based image. (D) is the spectrum curve of three ROIs in metastatic lymph node. The shapes of spectrum curves are similar to each other.

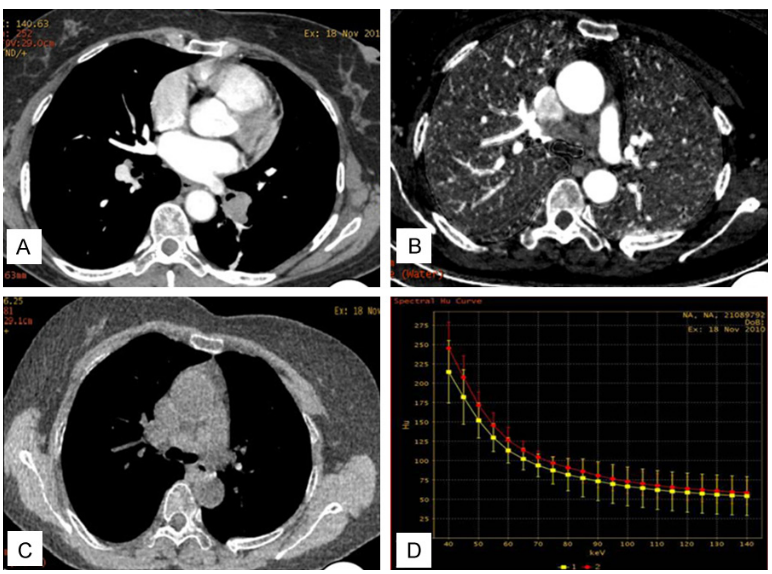

Figure 3. A 56 year old female with LAC. (A) is an enhanced axial monochromatic image of the chest showing fused lymph nodes from peripheral lung cancer. (B) and (C) are an iodine-based image and a water-based image. Metastatic lymph nodes are more obvious on the iodine-based image than on the water-based image. (D) is the spectrum curve of three ROIs in metastatic lymph node. The shapes of spectrum curves are similar to each other.

scan parameters: 120 kVp, auto mA, thickness = 5.0 mm, interval = 5.0 mm, and pitch = 1.375. The contrast-enhanced scan in the arterial phase was acquired using the spectral imaging mode with single-source, fast tube voltage switching between 80 and 140 kVp. The other scan parameters were: 600 mA, thickness = 5.0 mm, interval = 5.0 mm, pitch = 0.984, 39.37 mm/cycle rotation speed and 0.8s rotation time.

For the spectral CT imaging, two types of images were reconstructed using a single spectral CT scan: monochromatic image sets and material decomposition image sets. These images included 11 sets of monochromatic images with energy levels from 40-140 keV in 10 keV intervals and material decomposition images using iodine and water as the base material pair. Images were sent to an AW4.4 workstation for analysis after reconstructed to a thickness of 0.63 mm. The CT attenuation values and their standard deviations for the lymph nodes and surrounding parenchyma were measured, and contrast-noise-ratios for lymph node were generated in the 11 sets of monochromatic images. The iodine and water contents were measured in the iodine and water-based images, respectively. The monochromatic image set, where the best contrast noise ratio was recorded, was used to observe the metastatic lymph nodes. The attenuation curves in three different regions of interest (ROIs) in the arterial phase images at different keV levels were obtained.

Statistical analysis

All the statistical analyses were performed using SPSS19.0 (SPSS Inc., Chicago, IL). The CT values of metastatic lymph nodes in different

Table 1. CNR of different single energy image with multiple Kev ($\overline{x}\pm s$)

Kev	40	50	60	70	80	90	100	110	120	130	140
CNR	0.69±0.34	0.72±0.21	0.78±0.21	0.81±0.20	0.73±0.18	0.50±0.17	0.43±0.15	0.41±0.23	0.39±0.13	0.37±0.26	0.36±0.03

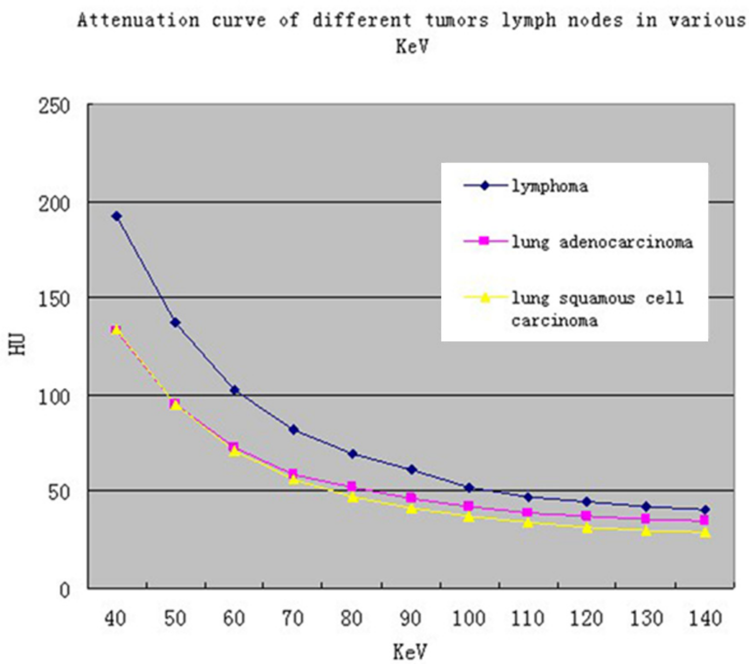

Figure 4. The attenuation curves of different malignant lymph nodes under a spectrum of Kev. The attenuation curves of LAC and LSC are different from that of Ly.

keV levels were analyzed using ANOVA followed with a Tamhane test. The content of iodine and water was compared using a T-test. A *P*-value of less than 0.05 was considered to indicate a statistically significant difference.

Results

Lymphadenopathy was found in Ly, LAC and LSC (**Figures 1A**, **2A** and **3A**). Images at 70 keV provided the highest CNR for lymph nodes and were used for visual image analysis (**Table 1**). The metastatic lymph nodes had higher contrast in iodine-based images with clearer boundaries than water-based images (**Figures 1B**, **1C**, **2B**, **2C**, **3B**, **3C**). With the increase of voltage, the attenuation of different ROI value decreased (**Figures 1D**, **2D** and **3D**). The attenuation curve of different metastatic lymph node tumors was different from each other except for LAC and LSC (**Figure 4**).

The CT attenuation values of metastatic lymphadenopathy at the 11 keV levels were different from each other ($P < 0.05$) (**Table 2**). At 70 keV, The CT attenuation values of metastatic lymphadenopathy were 81.36±9.81 HU, 58.33±21.55 HU and 56.47±10.62 HU for Ly, LAC and LSC, respectively. The iodine contents of Ly, LAC and LSC were (1.93±0.04), (1.16±0.15), and (1.25±0.21) g/L, respectively. The water contents of Ly, LAC and LSC were (1029.40±20.85), (1024.98±11.19) and (1022.12±12.94) g/L, respectively. The iodine contents of metastatic lymphadenopathy were different from each other ($P < 0.05$), except for LAC and LSC ($t = 1.77$, $P = 0.07$). There was no difference among the water contents of metastatic lymphadenopathy ($P > 0.05$) (**Table 3**).

Discussion

Lymph node metastasis is the most common metastatic pattern of lung cancer. Lymphoma is characterized by lymphadenectasis. Metastatic lymph nodes should have biological features similar to their original malignant tumor with similar cellularity, proliferative ratio, angiogenesis and tissue density in CT [10-13]. In conventional CT, the size, shape, and CT value of a lymph node is used to identify benign and malignant lymph nodes. Due to the limited spatial resolution for lymph nodes and the averaging effects of the polychromatic X-ray source in the conventional CT, the sensitivities and specificities of conventional CT in detecting metastatic lymph nodes ranged are fairly low, and limit the usage of conventional CT in the N-stage of lung cancer [17-20]. By applying two different kV setting simultaneously, dual energy CT is capable of generating a series of monochromatic images corresponding to photon energy levels from 40 keV to 140 keV, thus

Table 2. The CT values (HU) of different metastatic lymph nodes with multiple KV

KvP \ Tumor	LY	LC	LSC	*F*	*P*
40	193.08±32.48	132.44±58.5	133.60±40.61	12.08	0.00
50	136.64±21.43	94.63±39.98	94.67±25.32	13.11	0.00
60	102.38±14.19	72.29±29.85	70.82±16.10	8.61	0.00
70	81.36±9.81	58.33±21.55	56.47±10.62	17.29	0.00
80	69.68±69.68	51.81±19.65	46.63±7.00	18.97	0.00
90	60.92±4.61	45.99±17.28	41.20±5.78	18.02	0.00
100	51.70±6.49	41.93±15.73	36.99±5.00	10.04	0.00
110	47.39±6.22	39.08±14.71	33.85±4.88	9.18	0.00
120	44.39±5.81	37.08±14.03	31.64±31.63	8.66	0.00
130	41.99±5.69	35.53±13.57	30.01±5.12	7.94	0.00
140	40.12±5.61	34.31±13.20	28.70±5.27	7.4	0.00

**Tamhane* test was used due to heterogeneity of variance.

Table 3. Intergroup comparison of iodine and water in metastatic lymph nodes

Intergroup	Iodine-based		Water-based	
	T value	*P* value	*T* value	*P* value
Ly-LAC	26.29	0.00	1.11	0.31
Ly-LSC	16.81	0.00	1.48	0.14
LAC-LSC	1.77	0.07	0.86	0.39

providing images with better contrast resolution and additional information such as CT attenuation as a function of photon energy than conventional CT.

Our results indicate that there is a difference in the attenuation curves among the metastatic lymph nodes of different tumors. In the process of metastasis, normal lymph tissue is replaced by malignant tumor cells. The biological characteristics of lymph nodes are altered by metastasis, which leads to the observation of special attenuation curves. Metastatic lymph nodes are supposed to have similar micro-structures and densities to their original tumors. The small differences between the micro-structures and densities among various tumors are usually covered up by the averaging nature of the polychromatic X-ray in conventional CT. The monochromatic image sets generated in the dual energy spectral CT eliminated the averaging effect and the beam hardening effect associated with the polychromatic X-ray to produce more precise CT values and better contrast-to-noise ratios for lymph nodes and tumors to improving the assessment of this hidden information [21-23].

Blood supply is one of the most important factors of a tumor's biological behavior. Iodine content in the iodine-based images can be used to quantitatively measure the blood supply. The blood supply of lymph nodes from lymphoma is statistically higher than that of lymph nodes from lung adenocarcinoma and lung squamous cell carcinoma. The attenuation curve will be useful to decide the origin of lymph nodes. Our results are consistent with previous research where the blood supply of the inflammation is more than that of the malignant tumor [24, 25].

Limitations

GSI showed promising results in differentiating metastatic lymph nodes by way of quantitative information. However, the sample of this study was relative small. The sensitivity and specificity of GSI in differentiating metastatic lymph nodes is not provided. A larger sample and a ROC curve analysis are necessary in future studies.

Conclusion

Dual energy spectral CT imaging is a promising method for distinguishing metastatic lymph nodes from different malignant tumors using CT attenuation values at different photon energy levels and iodine content measurements.

Acknowledgements

This study was granted by National Natural Science Foundation of China (81171303), Shandong Provincial Natural Science Foundation of china (BS2012YY038, ZR2010HQ029 and ZR2009CL046) and Technology Development Plan (2010GSF10226), Weifang Science Project (20130167 and 201201242) and Affiliated Hospital of Weifang Medical University innovation fund project (K12QC1040). The research was also supported by project of

"Taishan Scholars Construction Engineering" and "Program for Scientific research innovation team in Colleges and universities of Shandong Province". The authors wish to thank Christopher Gothard for his help in English revision of this article.

Disclosure of conflict of interest

None.

Address correspondence to: Bin Wang, Department of Medical Imaging and Nuclear Medicine, Binzhou Medical University, 346 Guanhai Road, Laishan District, Yantai 264003, China. E-mail: binwang001@aliyun.com; Dr. Wenjuan Wang, Department of Radiology, Weifang People's Hospital, Weifang 261041, China. E-mail: wangwj212@163.com

References

[1] Lin XZ, Miao F, Li JY, Dong HP, Shen Y and Chen KM. High-definition CT gemstone spectral imaging of the brain: initial results of selecting optimal monochromatic image for beam-hardening artifacts and image noise reduction. J Comput Assist Tomogr 2011; 35: 294-297.

[2] Goo HW, Yang DH, Kim N, Park SI, Kim DK and Kim EA. Collateral ventilation to congenital hyperlucent lung lesions assessed on xenon-enhanced dynamic dual-energy CT: an initial experience. Korean J Radiol 2011; 12: 25-33.

[3] Watanabe Y. Deri vation of linear attenuation coefficients from CT numbers for low-energy photons. Phys Med Biol 1999; 44: 2201-2211.

[4] Lee YH, Park KK, Song HT, Kim S and Suh JS. Metal arte fact reduction in gemstone spectral imaging dual-energy CT with and without metal artifact reduction software. Eur Radiol 2012; 22: 1331-1340.

[5] Zhang D, Li X and Liu B. Objective characterization of GE discovery CT750 HD scanner: gemstone spectral imaging mode. Med Phys 2011; 38: 1178-1188.

[6] Deng K, Zhang CQ, Li W, Wang JJ, Wang XY, Pang T, Wang GL and Liu C. Preliminary application of high-definition CT Gemstone Spectral Imaging in hand and foot tendons. Korean J Radiol 2012; 1: 743-751.

[7] Wang G, Zhang C, Li M, Deng K and Li W. Preliminary application of high-definition computed tomographic gemstone spectral imaging in lung cancer. J Comput Assist Tomogr 2014; 38: 77-81.

[8] Srinivasan A, Parker RA, Manjunathan A, Ibrahim M, Shah GV and Mukherji SK. Differentiation of benign and malignant neck pathologies: preliminary experience using spectral computed tomography. J Comput Assist Tomogr 2013; 37: 666-672.

[9] Lee SH, Hur J, Kim YJ, Lee HJ, Hong YJ and Choi BW. Additional value of dual-energy CT to differentiate between benign and malignant mediastinal tumors: an initial experience. Eur J Radiol 2013; 82: 2043-2049.

[10] Kim AW. Lymph node drainage patterns and micrometastasis in lung cancer. Semin Thorac Cardiovasc Surg 2009; 21: 298-308.

[11] Monteiro R, Alfaro TM, Correia L, Simão A, Robalo Cordeiro C, Carvalho A and Costa JM. Mediastinal masses: case series. Acta Med Port 2011; 24: 899-904.

[12] Werewka-Maczuga A, Chrzan R, Urbanik A and Krochmalczyk D. Optimalisation of lymph node assessment in patients undergoing therapy for lymphoma using a multi-row CT. Przegl Lek 2010; 67: 256-261.

[13] Kodama K, Higashiyama M, Yokouchi H, Takami K, Kuriyama K, Mano M and Nakayama T. Prognostic value of ground-glass opacity found in small lung adenocarcinoma on high-resolution CT scanning. Lung Cancer 2001; 33: 17-25.

[14] Konishi J, Yamazaki K, Tsukamoto E, Tamaki N, Onodera Y, Otake T, Morikawa T, Kinoshita I, Dosaka-Akita H and Nishimura M. Mediastinal lymph node staging by FDG-PET in patients with non-small cell lung cancer: analysis of false-positive FDG-PET findings. Respiration 2003; 70: 500-506.

[15] Dwamena BA, Sonnad SS, Angobaldo JO and Wahl RL. Metastases from non-small cell lung cancer: mediastinal staging inthe1990s--meta-analytic comparison of PET and CT. Radiology 1999; 213: 530-536.

[16] Gould MK, Kuschner WG, Rydzak CE, Maclean CC, Demas AN, Shigemitsu H, Chan JK and Owens DK. Test performance of positron emission to mography and computed tomography for mediastinal staging in patients with non-small-cell lung cancer: ameta-analysis. Ann Intern Med 2003; 139: 879-892.

[17] Glazer GM, Gross BH, Quint LE, Francis IR, Bookstein FL and Orringer MB. Normal mediastinal lymph nodes: number and size according to American Thoracicociety mapping. AJR Am J Roentgenol 1985; 144: 261-265.

[18] Billè A, Okiror L, Skanjeti A, Errico L, Arena V, Penna D, Ardissone F and Pelosi E. Evaluation of integrated positron emission tomography and computed tomography accuracy in detecting lymph node metastasis in patients with adenocarcinoma vs squamous cell carcinoma. Eur J Cardiothorac Surg 2013; 43: 574-579.

[19] Billé A, Pelosi E, Skanjeti A, Arena V, Errico L, Borasio P, Mancini M and Ardissone F. Preoperative intrathoracic lymph node staging in patients with non-small-cell lung cancer: accuracy of integrated positron emission tomography and computed tomography. Eur J Cardiothorac Surg 2009; 36: 440-445.

[20] Yi CA, Lee KS, Kim BT, Shim SS, Chung MJ, Sung YM and Jeong SY. Efficacy of helical dynamic CT versus integrated PET/CT for detection of mediastinal nodal metastasis in non-small cell lung cancer. AJR Am J Roentgenol 2007; 188: 318-325.
[21] Zhang LJ, Yang GF, Wu SY, Xu J, Lu GM and Schoepf UJ. Dual-energy CT imaging of thoracic malignancies. Cancer Imaging 2013; 13: 81-91.
[22] Gupta RT, Ho LM, Marin D, Boll DT, Barnhart HX and Nelson RC. Dual-energy CT for characterization of adrenal nodules: initial experience. AJR Am J Roentgenol 2010; 194: 1479-1483.
[23] Li C, Zhang S, Zhang H, Pang L, Lam K, Hui C and Zhang S. Using the K-nearest neighbor algorithm for the classification of lymph node metastasis in gastric cancer. Comput Math Methods Med 2012; 2012: 876545.
[24] Yang ZG, Sone S, Takashima S, Li F, Honda T, Maruyama Y, Hasegawa M and Kawakami S. High-resolution CT analysis of small peripheral lung adenocarcinomas revealed on screening helical CT. AJR Am J Roentgenol 2001; 176: 1399-1407.
[25] Tateishi U, Nishihara H, Tsukamoto E, Morikawa T, Tamaki N and Miyasaka K. Lung tumors evaluated with FDG-PET and dynamic CT: the relationship between vascular density and glucose metabolism. J Comput Assist Tomogr 2002; 26: 185-190.